

Local Band Gap Measurements by VEELS of Thin Film Solar Cells

Debora Keller,^{1,2,*} Stephan Buecheler,¹ Patrick Reinhard,¹ Fabian Pianezzi,¹ Darius Pohl,³
Alexander Surrey,^{3,4} Bernd Rellinghaus,³ Rolf Erni,² and Ayodhya N. Tiwari¹

¹Empa—Swiss Federal Laboratories for Materials Science and Technology, Laboratory for Thin Films and Photovoltaics, Ueberlandstrasse 129, CH-8600 Duebendorf, Switzerland

²Empa—Swiss Federal Laboratories for Materials Science and Technology, Electron Microscopy Center, Ueberlandstrasse 129, CH-8600 Duebendorf, Switzerland

³Institute for Metallic Materials, IFW Dresden, P.O. Box 270116, D-01171 Dresden, Germany

⁴Institut für Festkörperphysik, TU Dresden, D-01062, Germany

Abstract: This work presents a systematic study that evaluates the feasibility and reliability of local band gap measurements of Cu(In,Ga)Se₂ thin films by valence electron energy-loss spectroscopy (VEELS). The compositional gradients across the Cu(In,Ga)Se₂ layer cause variations in the band gap energy, which are experimentally determined using a monochromated scanning transmission electron microscope (STEM). The results reveal the expected band gap variation across the Cu(In,Ga)Se₂ layer and therefore confirm the feasibility of local band gap measurements of Cu(In,Ga)Se₂ by VEELS. The precision and accuracy of the results are discussed based on the analysis of individual error sources, which leads to the conclusion that the precision of our measurements is most limited by the acquisition reproducibility, if the signal-to-noise ratio of the spectrum is high enough. Furthermore, we simulate the impact of radiation losses on the measured band gap value and propose a thickness-dependent correction. In future work, localized band gap variations will be measured on a more localized length scale to investigate, e.g., the influence of chemical inhomogeneities and dopant accumulations at grain boundaries.

Key words: VEELS, monochromated STEM, band gap, Cu(InGa)Se₂, chalcopyrite, solar cell

INTRODUCTION

Thin film solar cells based on Cu(In,Ga)Se₂ absorber layers have demonstrated high conversion efficiencies above 20% and therefore manifest a promising potential for the development of high efficiency, flexible, low-cost solar cells (Chirilă et al., 2013). However, despite the high efficiencies of Cu(In,Ga)Se₂ thin film solar cells, many fundamental properties that govern the performance are not yet clearly understood. Amongst other factors, compositional inhomogeneities strongly affect the efficiency as they directly influence the electro-optical properties of the Cu(In,Ga)Se₂ layer (Abou-Ras et al., 2011; Chirilă et al., 2011). In order to further improve the performance of Cu(In,Ga)Se₂ solar cells in a targeted way, a tool is sought that allows analysis of the optic and electronic properties on the nanoscale and to understand the underlying mechanisms caused by inhomogeneities in the Cu(In,Ga)Se₂ absorber layer.

Compositional gradients and inhomogeneities in Cu(In,Ga)Se₂, such as Cu and Ga concentration gradients, are formed during the fabrication process and can be tuned to a certain extent (Chirilă et al., 2011). In Ga-enriched zones, the conduction band minimum of Cu(In,Ga)Se₂ is pushed to

higher energies causing an enlargement of the band gap (E_g) from 1.0 eV (for CuInSe₂) to 1.7 eV (for CuGaSe₂) (Wei et al., 1998; Han et al., 2005; Chirilă et al., 2011). Likewise, a Cu depletion leads to an increase of the band gap. The Cu concentration, however, mainly affects the valence band maximum: because of decreased density of Cu 3d electrons, the repulsive interactions between Cu 3d and Se 4p electrons are reduced causing a lowering of the valence band maximum (Han et al., 2005; Minoura et al., 2013). For these reasons, the correlation between compositional effects and optical and electronic properties has been addressed within many studies, mainly using optical methods such as spectroscopic ellipsometry or vacuum ultraviolet spectroscopy (see, e.g., Van Benthem et al., 2001; Minoura et al., 2013). While these techniques reach high-energy resolutions (~2 meV), they suffer from limited lateral resolution, which is insufficient for investigating nanoscale inhomogeneities of electronic properties (Alonso et al., 2001; Gu et al., 2007; Minoura et al., 2013).

Valence electron energy-loss spectroscopy (VEELS) is a promising tool to probe local inhomogeneities with high lateral resolution down to the nanometer scale (Erni & Browning, 2005). The energy-loss function contains information about the joint density of unoccupied states above the Fermi level and material-specific collective plasmon excitations (Erni & Browning, 2005; Gu et al., 2007).

Received November 5, 2013; accepted February 23, 2014

*Corresponding author. debora.keller@empa.ch

However, the interpretation of VEEL spectra and the extraction of electronic properties, such as band gap and higher intra- and interband transition energies, require careful consideration. Various artifacts interfere with the VEEL spectrum depending on the probed material and the microscope used. The initial energy spread of the electron source, the nonisochromaticity of the spectrometer, the blurring of the detector, and instabilities of the microscope limit the energy resolution. Energy resolutions of around 0.2, 0.3, or 1.0 eV are reached, depending whether the microscope is equipped with a monochromated source, a cold-field emission gun, or a Schottky emitter, respectively (Erni & Browning, 2005; Aguiar et al., 2013). Aside from the instrumental factors, radiation and surface losses such as Cerenkov losses, the excitation of guided light modes, or surface plasmons may interfere with the energy-loss function that should be representative for “bulk” material. The presence and impact of these additional spectral contributions depend on the specimen thickness and the properties of the probed material, i.e., its refractive index and dielectric function (Kimoto et al., 2005; Gu et al., 2007; Erni & Browning, 2008).

Consequently, no standard procedure for band gap measurement by VEELS is generally applicable, but rather, each combination of microscope equipment, material question, and specimen characteristics will introduce its own specific problems. Accordingly, various strategies were proposed to extract band information from VEELS by different band gap studies reported in the literature (see, e.g., Rafferty & Brown, 1998; Schamm & Zanchi, 2003; Erni & Browning, 2005; Zhang et al., 2008).

In this work, a systematic approach to measure local band gap variations in Cu(In,Ga)Se₂ is presented, comparing

different strategies to extract the band gap energy from VEEL spectra. The feasibility and reliability of the band gap measurement by VEELS is discussed, based on error estimations and the comparison of the results with simulations. The results presented in this study are specific for the investigated material and the experimental setup. Nonetheless, our analysis allows for outlining general guidelines of the critical factors that impact the reliability of quantitative VEELS measurements.

MATERIALS AND METHODS

Solar Cell Processing and Transmission Electron Microscope (TEM) Specimen Preparation

The investigated high efficiency Cu(In,Ga)Se₂ solar cell was prepared according to the method presented by Chirilă et al. (2011) using a low temperature multistage coevaporation process to grow the absorber layer onto a flexible substrate. A transmission electron microscope (TEM) image of the layered structure of the Cu(In,Ga)Se₂ solar cell is shown in Figure 1a. The Cu and Ga relative concentrations across the Cu(In,Ga)Se₂ layer were measured by energy-dispersive X-ray (EDX) spectroscopy line profiles (Fig. 1b). Because the band gap increases at Ga-rich and Cu-poor regions, the band gap energy is expected to be highest at position 1 and lowest at position 2. At positions 3 and 4 intermediate band gap energies are expected, whereas the band gap energy at position 4 may be slightly higher than at position 3.

TEM samples were prepared from a completed Cu(In,Ga)Se₂ solar cell by mechanical polishing of cross-sections followed by Ar ion milling. The Fischione TEM ion mill 1050

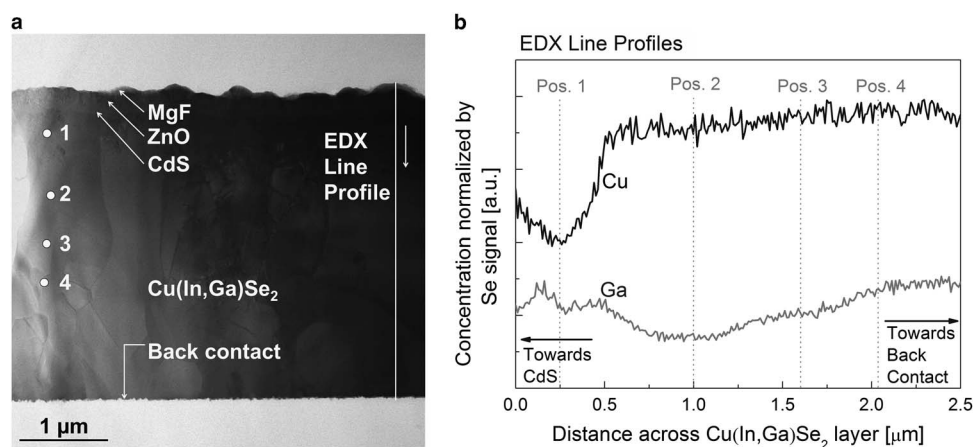


Figure 1. **a:** TEM cross-section image of a Cu(In,Ga)Se₂ solar cell. The full layer stack consists of the following layers: polyimide substrate and molybdenum back contact (both not visible in the micrograph)/absorber layer [Cu(In,Ga)Se₂, 2.5 μm]/*n*-type semiconductor (CdS, 0.04 μm)/bi-layered front contact (*i*-ZnO, ZnO:Al, 0.35 μm)/anti-reflection coating (MgF₂, 0.1 μm). The positions of the EDX and VEELS (1–4) acquisition locations are roughly estimated and sketched in the micrograph. **b:** Relative gallium and copper concentration variations across the Cu(In,Ga)Se₂ layer measured by EDX. Based on the EDX profiles, four positions across the Cu(In,Ga)Se₂ layer are chosen for band gap measurements, where maximal differences in the band gap energy are expected: the highest band gap energy is expected at position 1 (0.25 μm below the Cu(In,Ga)Se₂/CdS interface), the lowest at position 2 (1.00 μm below the interface), and intermediate band gap energies at positions 3 and 4 (1.60 and 2.05 μm below the interface, respectively). TEM, transmission electron microscope; EDX, energy-dispersive X-ray; VEELS, valence electron energy-loss spectroscopy.

(Fischione Instruments, Inc., Export, PA, USA) with liquid nitrogen cooling prevented the sample from overheating.

STEM (EDX) Analysis and VEELS Acquisition

EDX data were recorded on a JEOL 2200FS TEM/STEM (JEOL Ltd., Tokyo, Japan) operated at 200 kV. The intensity profiles of Cu and Ga in Figure 1b were normalized with respect to specimen thickness variations by the intensity profile of Se. This normalization is based on the assumption that the Se content is constant within the Cu(In,Ga)Se₂ layer.

VEEL spectra were recorded on a FEI (FEI, Eindhoven, The Netherlands) Titan3 TEM/STEM (FEI) operated at 300 kV. A Wien-type monochromator was used, providing an energy resolution of 140 meV as the full-width at half-maximum (FWHM) of the zero-loss peak (ZLP) for an exposure time of 1 s. For an exposure time of 10 s, which was used to acquire the spectra, the FWHM of the ZLP was enlarged to 240 meV. A dispersion of 30 meV/pixel was chosen. The convergence semi-angle of the electron probe was 10 mrad and the collection semi-angle was 2.5 mrad.

EDX and VEELS data were acquired on the same region of the specimen (see Fig. 1a). For VEELS analysis, four positions across the Cu(In,Ga)Se₂ layer thickness were selected at 250, 1,000, 1,600, and 2,050 nm depth with respect to the CdS/Cu(In,Ga)Se₂ interface (see Fig. 1a). A new reference ZLP in vacuum and a dark spectrum were acquired each time before recording low-loss spectra at a new site. Three subsequent low-loss spectra were acquired per site, with a small shift (<50 nm) of the beam after each acquisition to avoid contamination and beam damage effects.

BACKGROUND CORRECTION AND DATA PROCESSING

The ZLP was subtracted from the low-loss spectra by fitting the premeasured reference ZLP to the low-loss spectrum

using the software DigitalMicrograph by Gatan (Gatan Inc., Pleasanton, CA, USA). The subtraction included the following steps: first, a Gaussian function was fitted to both, the reference ZLP, and the ZLP in Cu(In,Ga)Se₂, in order to find their maximum points. Next, the two spectra were aligned by sub-channel interpolation according to the maxima of the fitted Gaussian functions. Finally, the reference ZLP was scaled by an appropriate scaling factor and subtracted from the low-loss spectrum. The scaling factor was calculated by the intensity ratio between the two ZLPs in a defined energy range. In order to check the importance of the chosen range, the results after background corrections using different fit ranges were compared. It was found that the closer the fit range approaches the band gap, the more accurate the background correction becomes. Nevertheless, the considered energy range must not overlap with the band gap energy. Thus, a fit range of 0.2–0.9 eV was chosen for the current study, as the band gap of the investigated Cu(In,Ga)Se₂ layer was expected to be larger than 1.0 eV at every investigated position. It should be noted that the optimal background correction parameters could only be defined with prior knowledge about the material and the approximate band gap region. In Figure 2, the raw spectrum and the ZLP subtraction are shown as examples for (a) a spectrum with a high signal-to-noise ratio (SNR) and (b) a spectrum with a lower SNR.

The noise in the background corrected spectra was reduced by a Savitzky–Golay smoothing filter (second-order polynomial). To extract the band gap energy by a parabolic fit, either no filter or the Savitzky–Golay filter at low or high strength was applied, considering surroundings of 21 or 61 points, equivalent to 0.6 or 1.8 eV. For the band gap extraction by the inflection point method, the Savitzky–Golay filter was applied for surroundings of 41 points, equivalent to 1.2 eV. In order to check the influence of the noise filtering, fast Fourier transformation filters and adjacent average filters were also applied at different strengths. In general, the choice of filter type and strength only slightly affected the obtained

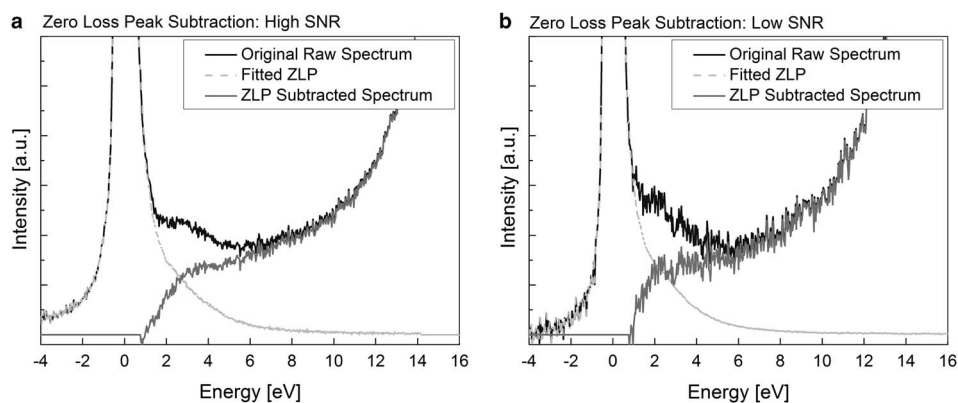


Figure 2. The ZLP was subtracted from the original low-loss spectrum by use of a premeasured, fitted reference ZLP. As an example, the original spectrum, the subtracted ZLP, and the remaining spectrum after the ZLP subtraction are exemplarily shown for a spectrum with high SNR (a) and for a spectrum with low SNR (b). In the latter case, the high noise level in the spectrum generates artifacts during the band gap extraction procedure and therefore hampers a proper band gap energy extraction. ZLP, zero-loss peak; SNR, signal-to-noise ratio.

band gap result, provided that the original spectrum showed a high SNR. However, starting from spectra with a low SNR, such as the spectrum given in Figure 2b, the choice of filter strongly influenced the band gap results. Therefore, a high SNR (see Results and Discussion section) was considered as prerequisite for reliable band gap measurement.

Simulations of VEEL spectra and scattering plots were based on the dispersion-bracket formalism proposed by Bolton & Chen (1995), considering normal incidence on single- or multilayered samples. The dispersion-bracket formalism of Bolton and Chen is equivalent to the Kröger formula, but expandable to multilayered systems (Kröger, 1968; Erni et al., 2008). The dielectric function of $\text{Cu}_{0.91}\text{In}_{0.57}\text{Ga}_{0.43}\text{Se}_2$, which was experimentally determined by Minoura et al. (2013) by means of ellipsometry, was used as input for the simulations.

Band Gap Extraction Strategies

Two different routes were used to extract band gap energies from the low-loss spectra, namely the parabolic fit and the inflection point approach.

Based on the work of Batson et al. and Rafferty and Brown, the VEEL spectrum reflects the joint density of states, which is described by a parabolic shape at a direct band gap. Therefore, they proposed to fit a parabola $(E - E_g)^{1/2}$ to the onset in the spectrum in order to find the band gap energy at the intersection of the parabola with the energy axis (Batson et al., 1986; Bangert et al., 1998; Rafferty & Brown, 1998; Erni & Browning, 2005). This approach has been used to measure band gaps on $\text{Cu}(\text{In,Ga})\text{Se}_2$. Two different, individually chosen fit ranges have been applied on each spectrum to fit the parabola. A parabolic fit to a low-loss spectrum is exemplarily sketched in Figure 3a.

Another way to assess the band gap energy was proposed by Lazar et al., defining the band gap energy as the energy at the inflection point of the rising intensity in the

low-loss spectrum (Lazar et al., 2003; Specht et al., 2005; Erni & Browning, 2007). In order to measure the band gaps by this route, three different ways to determine the inflection point were used for each spectrum. Starting from the first derivative of the smoothed spectrum, the inflection point was found at (i) the direct maximum of the derivative, (ii) at the maximum of the smoothed derivative, or (iii) at the maximum of a Gaussian curve that was fitted to the derivative (Fig. 3b).

RESULTS AND DISCUSSION

Comparison of the Band Gap Extraction Strategies

The results obtained by the parabolic fit approach include different error contributions. The errors stemming from the individual contributions, namely the choice of the parabolic fit range (E_R), the choice of smoothing filter (E_F), and the acquisition reproducibility (E_A), are individually evaluated (Fig. 4a). The errors are calculated as standard deviations of the results if (i) two different fit ranges (E_R), (ii) three different smoothing strengths (E_F), and (iii) three measurement repetitions (E_A) are applied. The total errors (E_T) are calculated by the formula: $E_T = (E_R^2 + E_F^2 + E_A^2)^{0.5}$, based on the approximation that the individual error contributions are independent of each other to keep the treatment simple. Interestingly, except for the results at position 3, the largest error contribution originates from the acquisition reproducibility and not from the fitting procedure.

When using the inflection point approach, the individual errors originating from the acquisition reproducibility (E_A) and how the inflection point is defined (E_I) are determined (Fig. 4b). Here, the errors are calculated as standard deviations of the results if (i) three different inflection point determination strategies (E_I), and (ii) three measurement repetitions (E_A) are applied. The total error (E_T) is obtained by the formula: $E_T = (E_I^2 + E_A^2)^{0.5}$, assuming again, that the

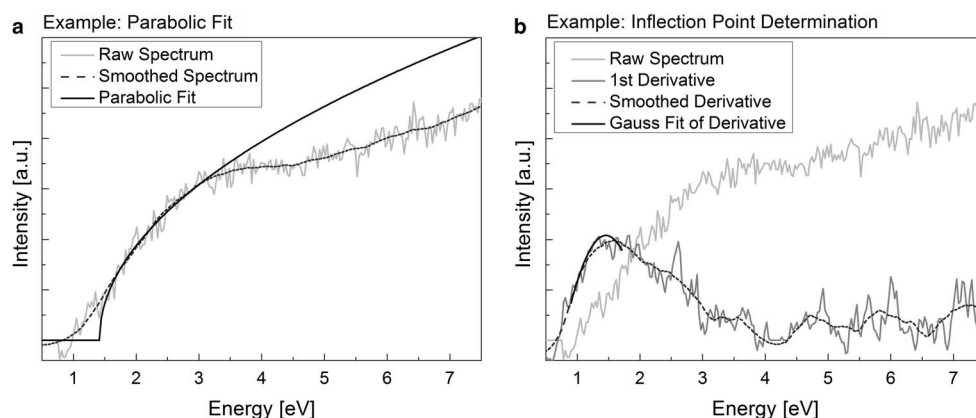


Figure 3. Two strategies to extract the band gaps from the low-loss spectra were applied: the parabolic fit (a) and the inflection point approach (b). In (a), a parabola is fitted to the spectrum to find the band gap at the intersection of the parabola and the energy axis. The parabola is fitted using different fit ranges and smoothing procedures of the spectrum. The inflection point in (b) is either determined as the maximum of the derivative, the maximum of the smoothed derivative, or by the maximum of a Gaussian fit to the derivative.

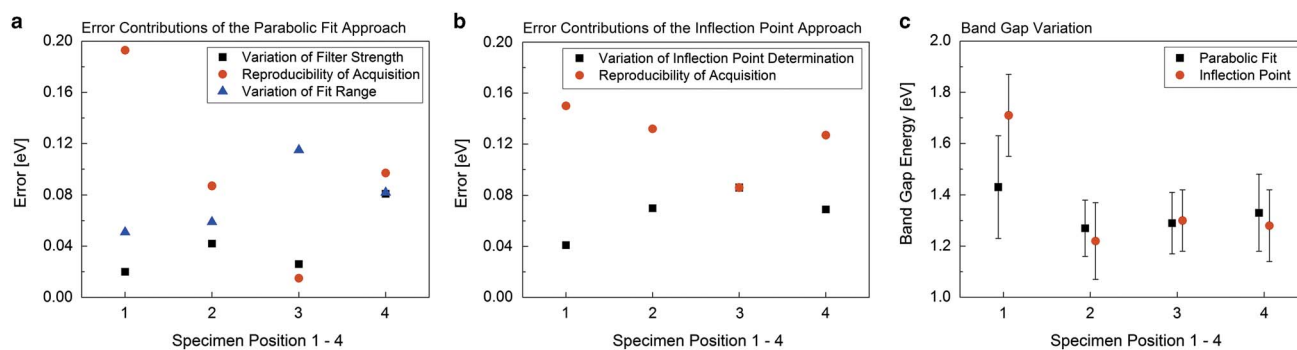


Figure 4. The individual error contributions are sketched for both approaches: parabolic fit (a) and inflection point (b). The errors in (a) are deduced for “Variation of Fit Range” from two values, for “Variation of Filter Strength” from three values (unfiltered, two filter strengths), and for “Reproducibility of Acquisition” from three values (i.e., three different measurements). The errors in (b) are deduced for “Variation of Inflection Point Determination” from three values (determination of the inflection point (i) at the direct maximum of the derivative, (ii) at the maximum of the smoothed derivative, or (iii) at the maximum of a Gaussian curve that was fitted to the derivative), and for “Reproducibility of Acquisition” from three values (i.e., three different measurements). In (c), the band gap values at the four positions (1–4) in the Cu(In,Ga)Se₂ layer are determined by two different approaches: fitting a parabola to the onset in VEELS and determining the inflection point on the onset as band gap. The given error bars represent the total errors.

individual error contributions are uncorrelated. The error contributions because of the acquisition reproducibility are similar as with the parabolic fit method and again, the error contributions stemming from the evaluation procedure are smaller than the errors stemming from acquisition reproducibility.

In Figure 4c, the results of the band gap energy measurements at the four positions in Cu(In,Ga)Se₂ are sketched for both data analysis methods. The error bars represent the total errors as defined above.

Comparing the two approaches, both reveal the same trend in the band gap variation within the Cu(In,Ga)Se₂ layer. In contrast to positions 2–4, where the measured band gap energies only vary in a narrow range (<0.08 eV), a significantly higher band gap energy is found at the first position, which is the closest to the Cu(In,Ga)Se₂/CdS interface (Fig. 4c). This variation agrees well with the expectations based on the relative compositional gradients observed by EDX (Fig. 1b). The copper depletion and also the increased gallium concentration close to the interface both cause an enlargement of the band gap, which matches the relative variation detected by VEELS.

Considering the absolute band gap values obtained by VEELS, the two methods lead to different results. Especially at the first position, the inflection point approach reveals a significantly higher value than the parabolic fit method. A similar discrepancy has been observed by, e.g., Lazar et al. (2003) and Specht et al. (2005), which was explained by defects and surface states in the specimen that cause some intensity below the band gap and shift the values measured by parabolic fits to lower energies. However, in the present case, optical and electrical measurements result in lower band gap energies compared with the VEELS results: band gap extraction from the Cu(In,Ga)Se₂ absorption edge in our external quantum efficiency (EQE) measurements revealed a band gap of 1.13 eV, assuming a direct band gap of the

absorber layer and that the EQE is proportional to the absorption coefficient (Hegedus & Shafarman, 2004). Further, the band gap extraction from our temperature-dependent short circuit current density versus open circuit voltage measurements revealed a band gap of 1.17 eV by extrapolating the open circuit voltage to a temperature of 0 K, according to the procedure described by Nadenau et al. (2000). As these methods measure the band gap in different ways and at different layer depths, the values cannot directly be compared with the VEELS results. Considering the present measurements by VEELS, the absolute values shift depending on the band gap extraction strategy. Therefore, the accuracy of VEELS concerning the absolute value is limited, and the error bars given here reflect the precision of the measurements regarding relative band gap variations.

Thickness Effects and Correction

The VEELS measurements were carried out at an acceleration voltage of 300 kV. First, one has to mention that radiation losses related to the retardation of the electrons are always present in VEELS data of a dielectric material, independent from whether the data are recorded with electrons above or below the Cerenkov threshold. Second, considering the fact that radiation losses increase with increasing electron energy, the interpretation of the VEELS data need to be considered with some care. However, the radiation losses enhance the signal at the band gap onset as the dielectric function is peaked there. This is beneficial in order to artificially enhance the band gap signal. On the other hand, the band gap onset might be shifted toward lower energies because of the radiation losses. Although the “artificial” amplification of the band gap signal because of the retardation effect at higher primary electron energies impairs the measurement of absolute values of the band gap, relative shifts can still precisely be measured. In any case, simulations of VEELS spectra are

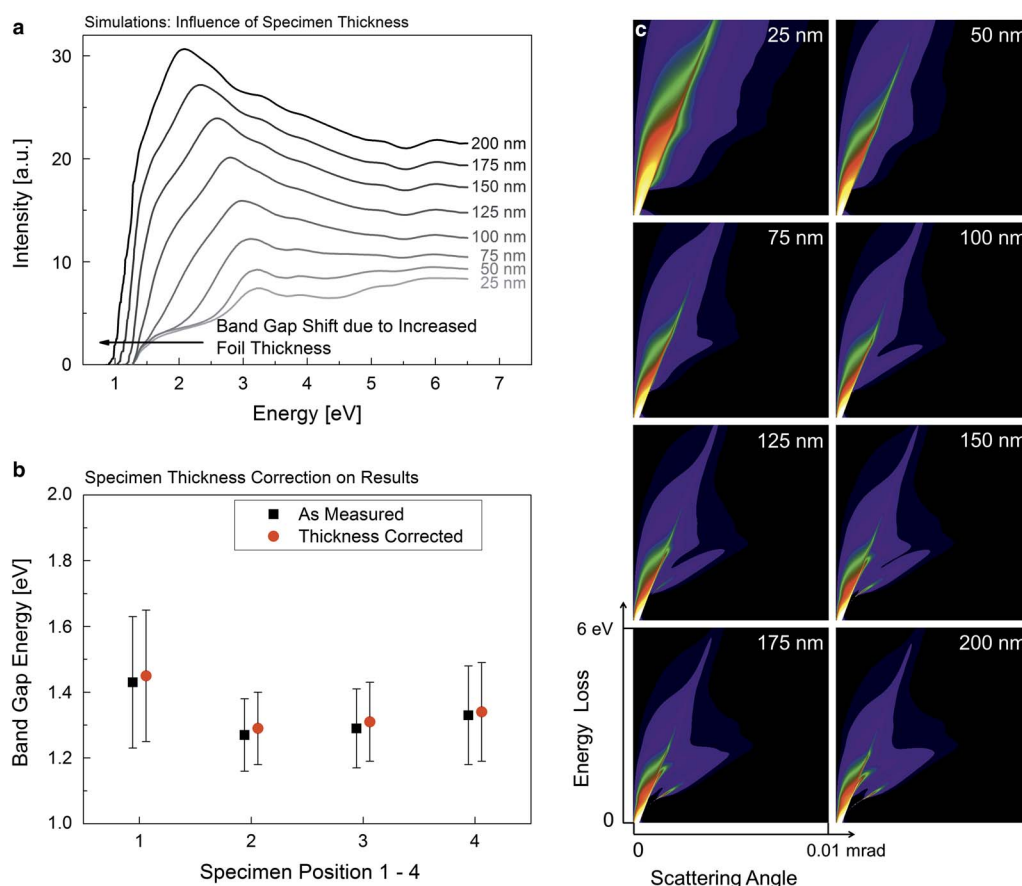


Figure 5. **a:** Simulated low-loss spectra for increasing foil thickness of 25–200 nm. The onset of the band gap signal shifts to lower energies by increasing thickness. **b:** The band gap energies, which are determined by parabolic fits, are corrected for thickness effects by thickness-dependent energy shifts estimated by simulations. However, in case of the present study, the correction is small, i.e., ~ 0.02 eV, as the specimen area is thin (roughly 50 nm). **c:** Simulated scattering diagrams of $\text{Cu}_{0.91}(\text{In}_{0.57}, \text{Ga}_{0.43})\text{Se}_2$ showing the energy loss probability in dependence of the scattering angle for increasing foil thickness of 25–200 nm. The scattering diagrams of $\text{Cu}_{0.91}(\text{In}_{0.57}, \text{Ga}_{0.43})\text{Se}_2$ indicate that Cerenkov losses and guided light modes only contribute significantly to the low-loss spectrum if the specimen is thicker than 100 nm.

mandatory to evaluate the significance of radiation losses, independent of the primary electron energy.

The simulated low-loss spectra of $\text{Cu}_{0.91}(\text{In}_{0.57}, \text{Ga}_{0.43})\text{Se}_2$ for different specimen thicknesses are given in Figure 5a. Energies at the onsets of the simulated spectra were considered as band gap. The simulations show that the band gap signal decreases with the specimen thickness. This decay of the measurable band gap can be approximated with a linear function according to the empirical formula:

$$E_{g \text{ measured}} [\text{eV}] = E_{g \text{ true}} [\text{eV}] - 0.0004 \times \left[\frac{\text{eV}}{\text{nm}} \right] \times \text{thickness}_{\text{specimen}} [\text{nm}].$$

Using this relation, the experimental results are corrected for thickness effects. However, in the presented measurements, the effect is weak as the investigated area is thin, i.e., roughly 50 nm as measured by the EELS log-ratio method (Malis et al., 1988). The band gaps as measured by the parabolic fit approach and the corresponding thickness corrected values are shown in Figure 5b.

The simulated scattering diagrams of $\text{Cu}_{0.91}(\text{In}_{0.57}, \text{Ga}_{0.43})\text{Se}_2$ sketch the expected energy-loss contributions for increasing sample thickness. In the simulation for a specimen thickness of 25 nm, the dominant feature is the light line. For specimens thicker than 100 nm, an additional branch is visible that shows the appearance of guided light modes. Therefore, on the described experimental conditions (see Introduction section), radiation losses only become apparent in $\text{Cu}_{0.91}(\text{In}_{0.57}, \text{Ga}_{0.43})\text{Se}_2$ for specimens thicker than 100 nm. However, as the specimen thickness of the sample is only around 50 nm, and the composition is assumed to be similar to the one used for the simulation, artifacts because of retardation effects are considered to be insignificant in the present case (Fig. 5c).

Comparative Discussion of the Reached Precision and Accuracy

In order to estimate the reliability of band gap measurement by VEELS in terms of precision and accuracy, mainly three groups of error sources are taken into account: first, an error

is introduced by the acquisition reproducibility; second, during data processing, and third, by interpretation of the results and subsequent correction for thickness and retardation effects.

Considering the precision of the presented results, the acquisition reproducibility yields the largest error. The deviations between subsequent measurements may on one hand stem from instabilities of the microscope (see Introduction section) and shot noise, and on the other hand from irregularities in the probed area, i.e., because of sample alteration by beam damage and contamination or because of intrinsic nanoscale inhomogeneities. As the beam was shifted after each measurement, it cannot be ruled out, that the probed spots might have been sensitive to local inhomogeneities, causing deviations in the band gap measurement.

The error contributions introduced during data processing are mainly governed by the quality of the spectrum, i.e., the SNR. In order to improve the SNR, a high acceleration voltage was used in this study and in this way, a SNR of about 5–6 just above the band gap signal was reached. As can be seen from the results, this value has to be considered as a lower limit. In spectra showing poorer SNR (not shown), the choice of smoothing procedure crucially influences the result. Further, the band gap extraction becomes very sensitive to the choice of fit range. Therefore, when spectra of poor SNR were considered, data processing caused large error contributions and the expected correlations between band gaps and chemical gradings were not found.

The impact of retardation effects on the precision of the measurement is estimated by simulations, which in practice implies that the dielectric response of the material is available. In case of structural defects such as interfaces, this condition may be critical, as the chemical composition of the material at the defect may deviate from the bulk composition and therefore the dielectric response of the material may be altered. In the present measurements of bulk material, however, the dielectric response of the material is assumed to be similar to the dielectric response of homogeneous $\text{Cu}_{0.91}(\text{In}_{0.57}\text{Ga}_{0.43})\text{Se}_2$ in all probed sample positions. Based on the results of the simulations for $\text{Cu}_{0.91}(\text{In}_{0.57}\text{Ga}_{0.43})\text{Se}_2$, the effect of retardation losses is small within the thickness range of our specimen (<100 nm). In addition, for all measurements, similar specimen thicknesses were used. Therefore, it is assumed for our measurements, that the retardation effects mainly impact the absolute values but not the relative variations and hence that the influence of retardation effects on the precision is negligible.

In summary, the precision of both band gap extraction techniques (parabolic fit and inflection point method) is mainly limited by the acquisition reproducibility and the SNR of the spectrum. In the presented case, the two methods both reach sufficient precision to detect the expected relative band gap variations. The absolute values are higher than expected based on optically and electrically determined band gap energies. As shown in this study, the interpretation of the spectra is critical for assessing the correct band gap values, however, relative shifts can be measured reliably.

CONCLUSIONS

In this work the feasibility and reliability of local band gap measurements on $\text{Cu}(\text{In,Ga})\text{Se}_2$ by VEELS is investigated. Besides the high-energy resolution, which is needed to resolve band gap signals down to 1 eV, a high SNR in the low-loss spectrum is also crucial to ensure reliable data processing and band gap measurements. Given that the SNR is high, the largest error afflicting the measured band gap energies is attributed to the acquisition reproducibility and not to signal processing and evaluation.

The band gap results, obtained by the two different band gap extraction techniques, both show roughly the same relative band gap variation that agrees well with expectations based on EDX data. Therefore, the relative band gap variations measured by VEELS are considered to be reliable despite the large error bars. However, the absolute values diverge depending on the used extraction technique. Thus, the absolute values have to be treated with care, even if the values lay within a reasonable range.

Simulations revealed that a slight shift of the band gap signal to lower energies is observed by increasing specimen thickness. A thickness correction is therefore applied on the results even though the effect is small on the used sample. Based on simulated scattering diagrams, critical retardation effects can be neglected for $\text{Cu}(\text{In,Ga})\text{Se}_2$ specimens thinner than 100 nm, i.e., for the presented results.

Conclusively, our VEELS measurements provide evidence for the band gap variations that can be expected based on EDX spectra. Thus, the results clearly prove the feasibility of relative band gap variation measurements by VEELS. As an outlook, more localized band gap variations, e.g., at grain boundaries, may be addressed in future to assess the feasibility and impact of concentration changes and dopant accumulations.

ACKNOWLEDGMENTS

Financial support from the Swiss National Science Foundation (SNF) is greatly acknowledged (Project No. 200020_132377). A.S. thanks the Reiner Lemoine Foundation for the generous financial support.

REFERENCES

- ABOU-RAS, D., CABALLERO, R., FISCHER, C.-H., KAUFMANN, C.A., LAUERMANN, I., MAINZ, R., MÖNIG, H., SCHÖPKE, A., STEPHAN, C., STRECK, C., SCHORR, S., EICKE, A., DÖBELI, M., GADE, B., HINRICH, J., NUNNEY, T., DIJKSTRA, H., HOFMANN, V., KLEMM, D., EFIMOVA, V., BERGMAIER, A., DOLLINGER, G., WIRTH, T., UNGER, W., ROCKETT, A.A., PEREZ-RODRIGUEZ, A., ALVAREZ-GARCIA, J., IZQUIERDO-ROCA, V., SCHMID, T., CHOI, P.-P., MÜLLER, M., BERTRAM, F., CHRISTEN, J., KHATRI, H., COLLINS, R.W., MARSILLAC, S. & KÖTSCHAU, I. (2011). Comprehensive comparison of various techniques for the analysis of elemental distributions in thin films. *Microsc Microanal* **17**, 728–751.
- AGUIAR, J.A., REED, B.W., RAMASSE, Q.M., ERNI, R. & BROWNING, N.D. (2013). Quantifying the low-energy limit and spectral resolution in valence electron energy loss spectroscopy. *Ultramicroscopy* **124**, 130–138.

- ALONSO, M.I., WAKITA, K., PASCUAL, J., GARRIGA, M. & YAMAMOTO, N. (2001). Optical functions and electronic structure of CuInSe_2 , CuGaSe_2 , CuInS_2 , and CuGaS_2 . *Phys Rev B* **63**, 075203.
- BANGERT, U., HARVEY, A., DAVIDSON, J., KEYSE, R. & DIEKER, C. (1998). Correlation between microstructure and localized band gap of GaN grown on SiC. *J Appl Phys* **83**, 7726.
- BATSON, P.E., KAVANAGH, K.L., WOODALL, J.M. & MAYER, J.W. (1986). Electron-energy-loss scattering near a single misfit dislocation at the GaAs/GaInAs interface. *Phys Rev Lett* **57**, 2729–2732.
- BOLTON, J.P.R. & CHEN, M. (1995). Electron energy loss in multilayered slabs. *Ultramicroscopy* **60**, 247–263.
- CHIRILĂ, A., BUECHELER, S., PIANEZZI, F., BLOESCH, P., GRETENER, C., UHL, A.R., FELLA, C., KRANZ, L., PERRENOUD, J., SEYRLING, S., VERMA, R., NISHIWAKI, S., ROMANYUK, Y.E., BILGER, G. & TIWARI, A.N. (2011). Highly efficient Cu(In,Ga)Se_2 solar cells grown on flexible polymer films. *Nat Mater* **10**, 857–861.
- CHIRILĂ, A., REINHARD, P., PIANEZZI, F., BLOESCH, P., UHL, A.R., FELLA, C., KRANZ, L., KELLER, D., GRETENER, C., HAGENDORFER, H., JAEGER, D., ERNI, R., NISHIWAKI, S., BUECHELER, S. & TIWARI, A.N. (2013). Potassium-induced surface modification of Cu(In,Ga)Se_2 thin films for high efficiency solar cells. *Nat Mater* **12**, 1107–1111.
- ERNI, R. & BROWNING, N.D. (2005). Valence electron energy-loss spectroscopy in monochromated scanning transmission electron microscopy. *Ultramicroscopy* **104**, 176–192.
- ERNI, R. & BROWNING, N.D. (2007). Quantification of the size-dependent energy gap of individual CdSe quantum dots by valence electron energy-loss spectroscopy. *Ultramicroscopy* **107**, 267–273.
- ERNI, R. & BROWNING, N.D. (2008). The impact of surface and retardation losses on valence electron energy-loss spectroscopy. *Ultramicroscopy* **108**, 84–99.
- ERNI, R., LAZAR, S. & BROWNING, N.D. (2008). Prospects for analyzing the electronic properties in nanoscale systems by VEELS. *Ultramicroscopy* **108**, 270–276.
- GU, L., SROT, V., SIGLE, W., KOCH, C., VAN AKEN, P., SCHOLZ, F., THAPA, S., KIRCHNER, C., JETTER, M. & RÜHLE, M. (2007). Band-gap measurements of direct and indirect semiconductors using monochromated electrons. *Phys Rev B* **75**, 195214.
- HAN, S.-H., HASOON, F.S., AL-THANI, H.A., HERMANN, A.M. & LEVI, D.H. (2005). Effect of Cu deficiency on the optical properties and electronic structure of $\text{CuIn}_{1-x}\text{Ga}_x\text{Se}_2$. *J Phys Chem Solids* **66**, 1895–1898.
- HEGEDUS, S.S. & SHAFARMAN, W.N. (2004). Thin-film solar cells: Device measurements and analysis. *Prog Photovolt* **12**, 155–176.
- KIMOTO, K., KOTHLEITNER, G., GROGGER, W., MATSUI, Y. & HOFER, F. (2005). Advantages of a monochromator for bandgap measurements using electron energy-loss spectroscopy. *Micron* **36**, 185–189.
- KRÖGER, E. (1968). Berechnung der Energieverluste schneller Elektronen in dünnen Schichten mit Retardierung. *Z Physik* **216**, 115–135.
- LAZAR, S., BOTTON, G.A., WU, M.-Y., TICHELAAR, F.D. & ZANDBERGEN, H.W. (2003). Materials science applications of HREELS in near edge structure analysis and low-energy loss spectroscopy. *Ultramicroscopy* **96**, 535–546.
- MALIS, T., CHENG, S.C. & EGERTON, R.F. (1988). EELS log-ratio technique for specimen-thickness measurement in the TEM. *J Electron Microsc Tech* **8**, 193–200.
- MINOURA, S., KODERA, K., MAEKAWA, T., MIYAZAKI, K., NIKI, S. & FUJIWARA, H. (2013). Dielectric function of Cu(In,Ga)Se_2 -based polycrystalline materials. *J Appl Phys* **113**, 063505–063505–14.
- NADENAU, V., RAU, U., JASENEK, A. & SCHOCK, H.W. (2000). Electronic properties of CuGaSe_2 -based heterojunction solar cells. Part I. Transport analysis. *J Appl Phys* **87**, 584.
- RAFFERTY, B. & BROWN, L. (1998). Direct and indirect transitions in the region of the band gap using electron-energy-loss spectroscopy. *Phys Rev B* **58**, 10326–10337.
- SCHAMM, S. & ZANCHI, G. (2003). Study of the dielectric properties near the band gap by VEELS: Gap measurement in bulk materials. *Ultramicroscopy* **96**, 559–564.
- SPECHT, P., HO, J.C., XU, X., ARMITAGE, R., WEBER, E.R., ERNI, R. & KISIELOWSKI, C. (2005). Band transitions in wurtzite GaN and InN determined by valence electron energy loss spectroscopy. *Solid State Commun* **135**, 340–344.
- VAN BENTHEM, K., FRENCH, R.H., SIGLE, W., ELSÄSSER, C. & RÜHLE, M. (2001). Valence electron energy loss study of Fe-doped SrTiO_3 and a $\Sigma 13$ boundary: Electronic structure and dispersion forces. *Ultramicroscopy* **86**, 303–318.
- WEI, S.-H., ZHANG, S.B. & ZUNGER, A. (1998). Effects of Ga addition to CuInSe_2 on its electronic, structural, and defect properties. *Appl Phys Lett* **72**, 3199–3201.
- ZHANG, L., ERNI, R., VERBEECK, J. & VAN TENDELOO, G. (2008). Retrieving the dielectric function of diamond from valence electron energy-loss spectroscopy. *Phys Rev B* **77**, 195119.